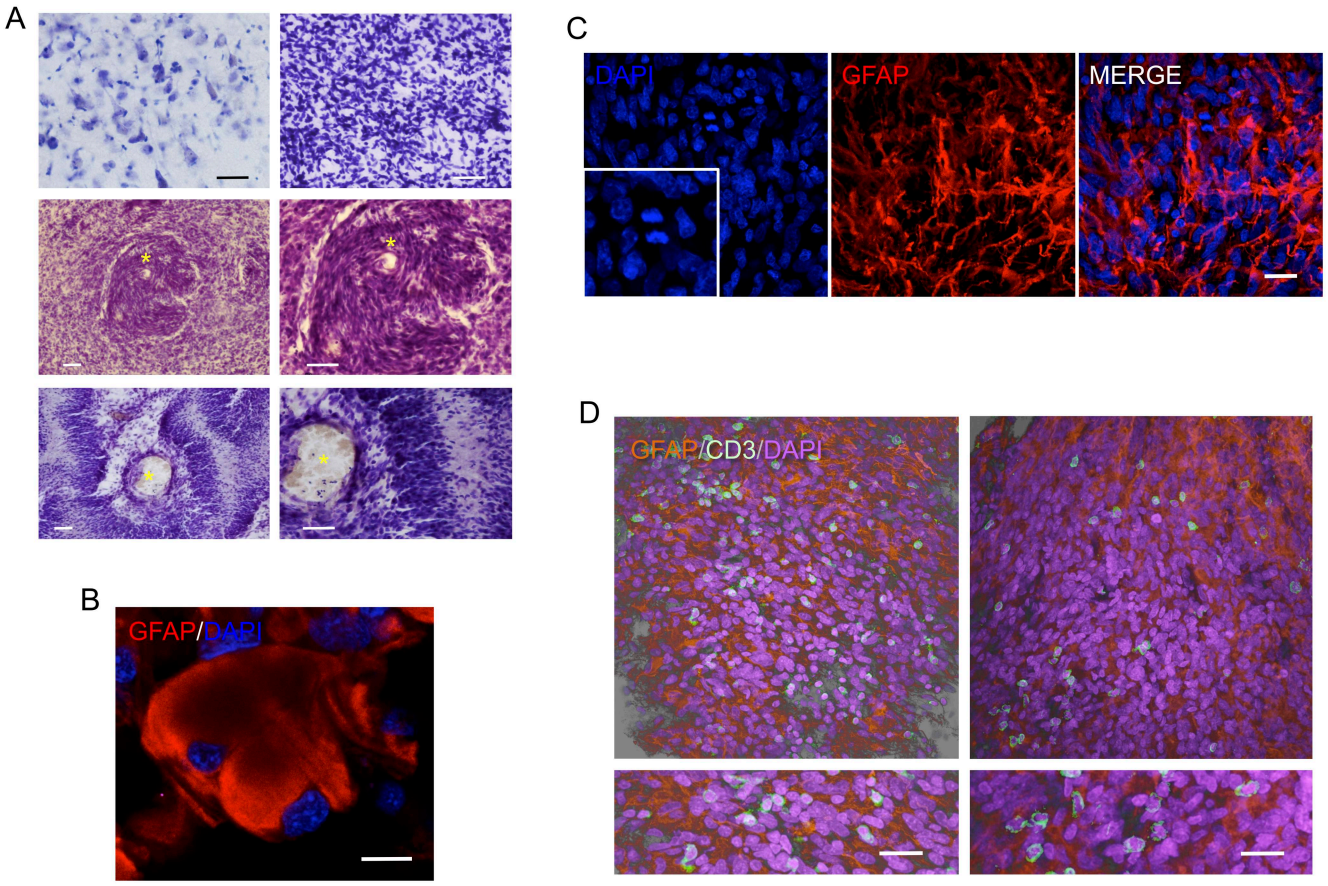

Figure S1. Samples revealed neuro-pathological characteristics of GBMs. A. Thionine-based Nissl staining shows classical features of GBM. In the top panel, normal human cortex (left) shows a typically well-organized architecture with even distribution of neurons and glia. However, cortical GBM (right) showed characteristic hyper-cellularity, hyper-chromatism and pleomorphism in a disorganized structure. Glomeruloid vessels were often seen in the tumors (middle panel) as well as distinctive necrotic pseudopalisades (bottom panel). Yellow asterisks indicate blood vessels. Scale bars: 50 μm. **B**. GBM samples show gemistocytic formations. Confocal image of a sample (Patient Grade IV) showing characteristic GFAP$^+$ cells (red) with swollen cytoplasm and lateralized nucleus (blue). Scale bar: 10 μm. **C**. GBM tumors show high density of nuclei (DAPI; blue) and fibrous GFAP staining (red). Aberrant mitoses were frequently seen (magnified in white box). Scale bar: 30 μm. **D**. Tumors are infiltrated by lymphocytes. Two cases of GBM, (left and right) are shown. GFAP$^+$ tumors (orange) present CD3$^+$ T cells infiltration (green). Counter staining was also performed with DAPI (magenta). Scale bars: 30 μm.

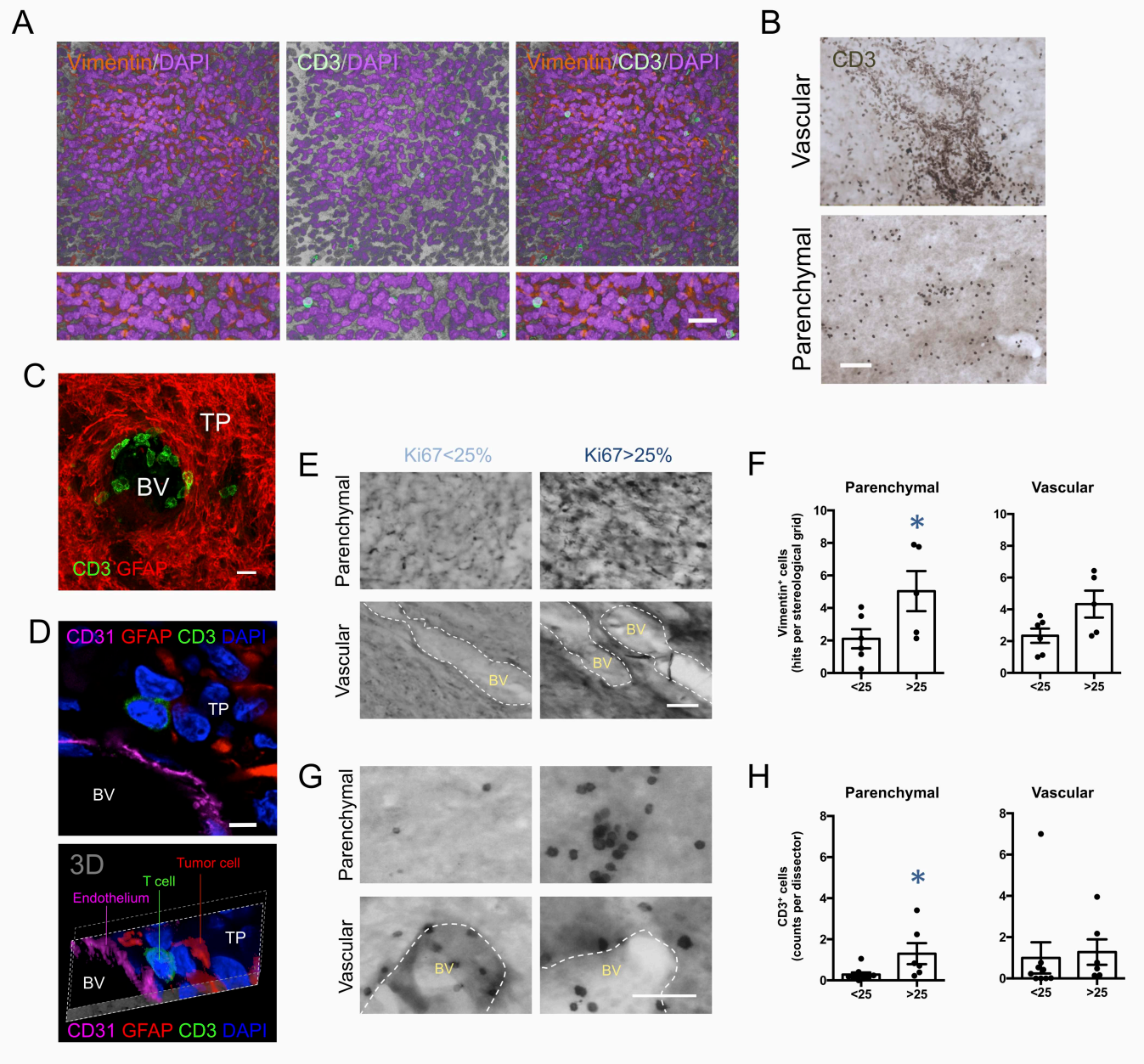

Figure S2. Biopsies of highly proliferative gliomas show higher T cell infiltration in the tumor parenchyma. A. 3D reconstruction of confocal scanning of biopsies demonstrates infiltration of $CD3^+$ T cells (light green) in the vimentin-rich (orange) and $DAPI^+$ poly-nucleated tumor areas (magenta). Scale bar: 30 μm. **B**. DAB immunostaining shows that T cells are distributed in vascular and parenchymal areas. Scale bar: 100 μm. **C**. Multi-labeling and confocal scanning show T cells in vascular lumina (BV) and homing in tumor parenchyma (TP). Scale bar: 10 μm. **D**. 3D reconstructions of confocal images show actual infiltration across the vascular endothelium. Scale bar: 5 μm. **E.**

Immunohistochemistry of vimentin$^+$ cells in human GBM in parenchymal and vascular areas according with the pathological diagnosis (% of Ki67). Scale bar: 50 μm. **F**. Stereological quantification of vimentin$^+$ cells according to Ki67 levels. A significant increase in vimentin$^+$ cells is seen in more aggressive gliomas. *p<0.05. **G**. Evidence, by immunohistochemistry of CD3$^+$ T cells in parenchymal and vascular (BV) areas. Scale bar: 50 μm. **H**. Highly proliferative gliomas show a significant increase of parenchymal T cell infiltration. *p<0.05 Student-t test.

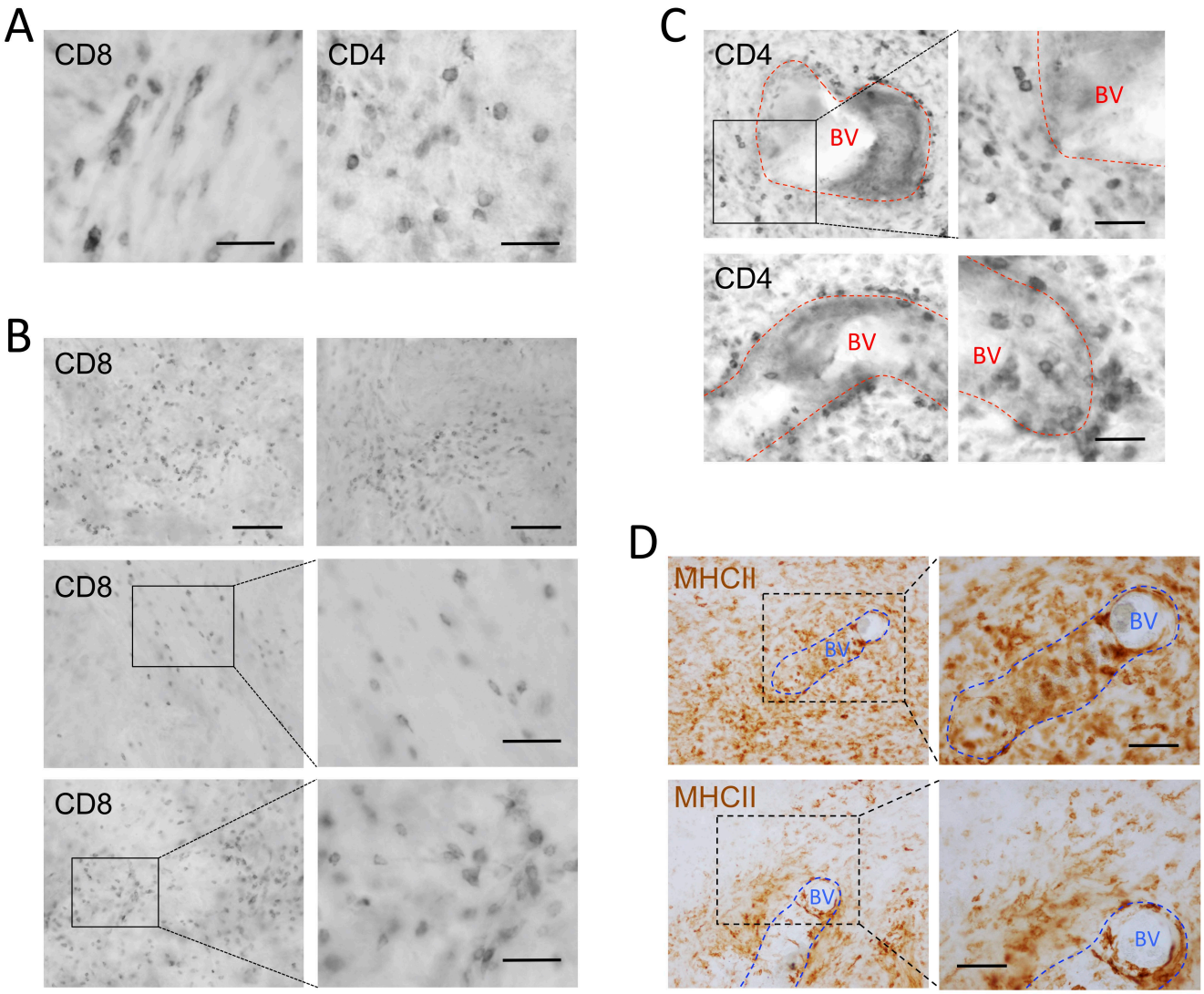

Figure S3. CD8⁺ and CD4⁺ T lymphocytes are present in human GBM. A. Both CD8⁺ and CD4⁺ T cells subsets can be seen in the TP of human GBM samples. Scale bars: 40 µm. **B.** CD8⁺ T cells are seen widely distributed along the tumorigenic parenchyma. Two examples are displayed with low magnification at the top panel. Scale bars: 80 µm. Two other examples showing higher magnifications from inserts are presented at the middle and bottom panel. Scale bars: 40 µm. **C.** CD4⁺ T cells are abundantly found in perivascular areas. Blood vessel (BV) limits are indicated by a red broken line. Scale bars: 40 µm. **D.** MHCII abundant areas are frequently found around tumorigenic blood vessels (BV). Two examples of perivascular stroma are shown. Higher magnifications of the inserts are displayed. Blood vessel (BV) limits are indicated by a blue broken line. Scale bars: 80 µm.

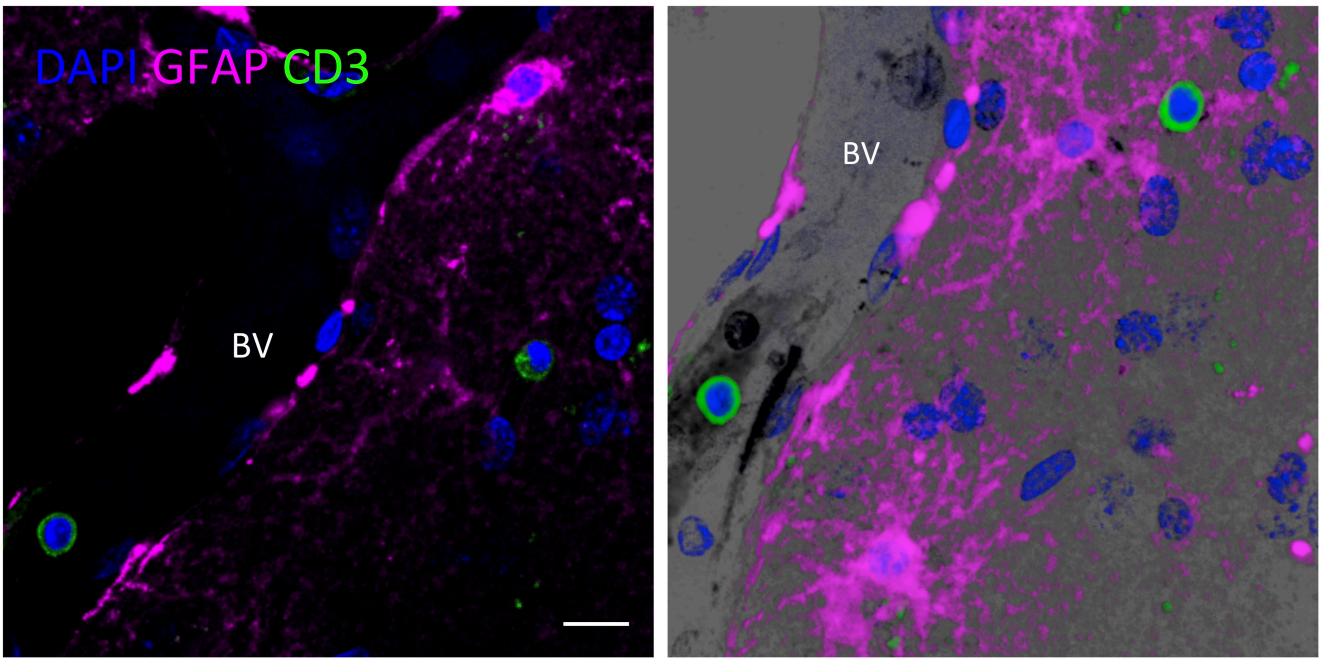

Figure S4. T-cells in non-malignant human cortex are relegated to BV or vascular surroundings. Confocal image of a non-malignant cortex showing the rare sighting of $CD3^+$ T cells (green) together with $GFAP^+$ perivascular astrocytes (magenta) and nuclear counterstaining (DAPI). Left image; optical section confocal image. Right image shows a three dimensional reconstruction at this tissue area. Scale bar 20 µm.

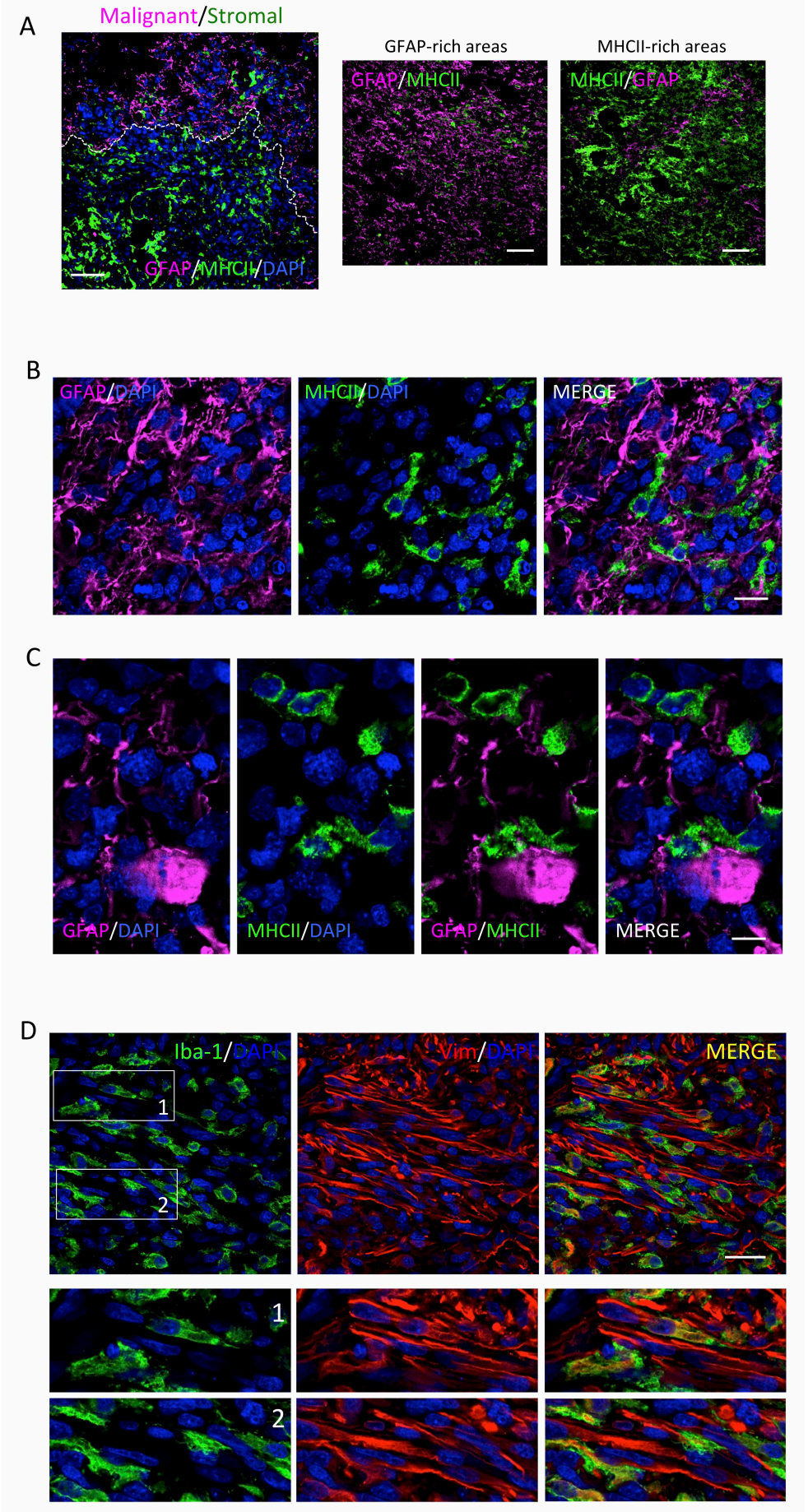
A
Malignant/Stromal
GFAP/MHCII/DAPI
GFAP-rich areas
GFAP/MHCII
MHCII-rich areas
MHCII/GFAP
B
GFAP/DAPI
MHCII/DAPI
MERGE
C
GFAP/DAPI
MHCII/DAPI
GFAP/MHCII
MERGE
D
Iba-1/DAPI
Vim/DAPI
MERGE
1
2
1
2

Figure S5. Malignant and stromal areas are distinguishable in GBM tissue. A. Staining with GFAP (magenta) was adequate to label malignant areas of the tumor whereas MHCII (green) staining labeled stroma. Both, GFAP-rich/MHCII-poor and MHCII-rich/GFAP-poor are discernible. Scale bars: 100 μm. **B.** $GFAP^+$ cells in the tumor do not show detectable levels of MHCII. Confocal images show a view of tumorigenic $GFAP^+$ area co-immunostained for MHCII. In the merged image, no expression of MHCII can be seen in $GFAP^+$ cells and vice versa. Scale bar: 20 μm. **C.** Zoom in and detail of the distinct expression of $GFAP^+$ cells and $MHCII^+$ cells. Scale bar: 10 μm. **D.** Microglia/macrophages in GBM express vimentin. Confocal images of the immunofluorescence for the microglial/macrophage marker Iba-1 (green) in combination with vimentin (red) show cells with clear co-expression of both markers. Bottom panels 1 and 2 are higher magnifications obtained from the top panel. Scale bar: 30 μm.

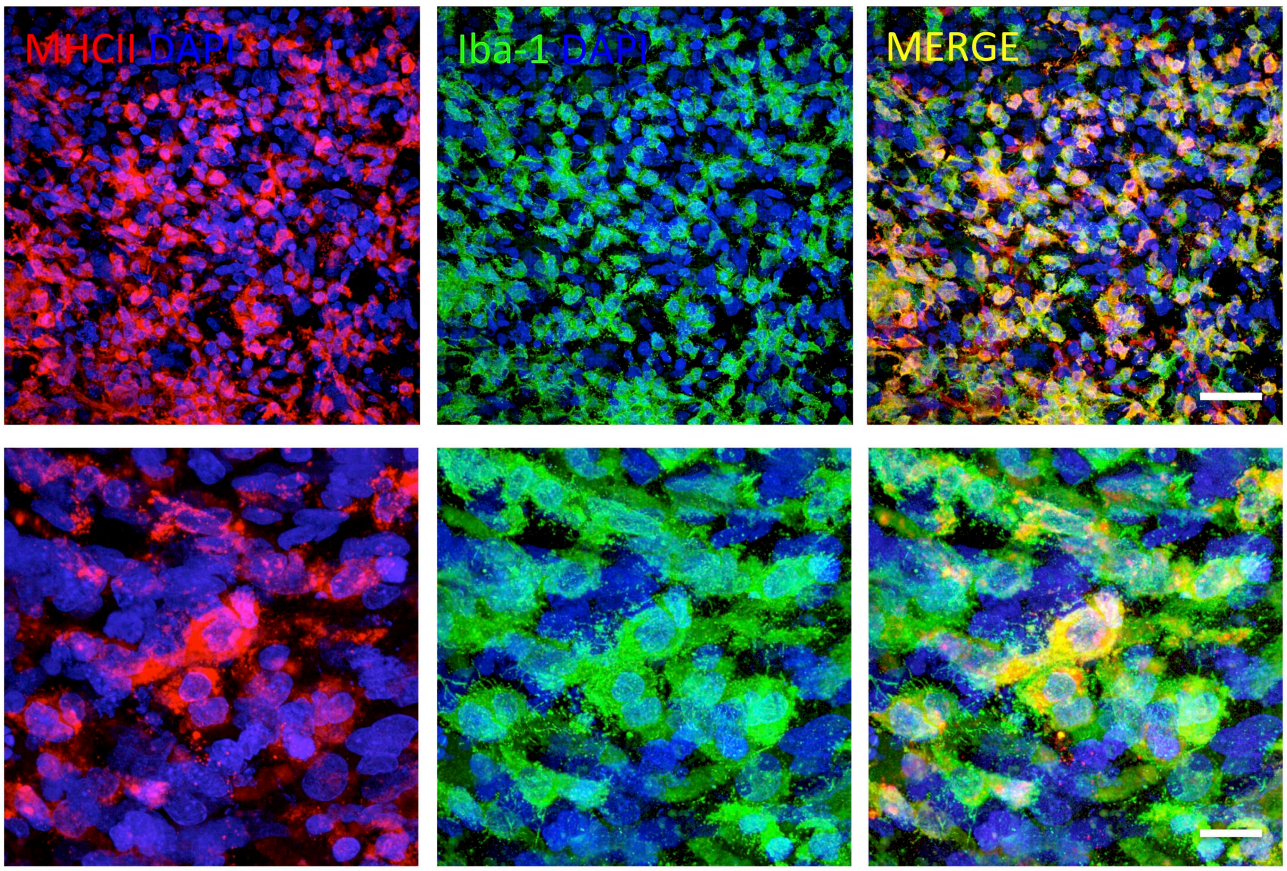

Figure S6. Human MHCII (HLADR) is expressed by microglia and brain infiltrated macrophages. Top panel shows a confocal scanning of a tissue block combining MHCII (red) and Iba-1 (green) markers, in addition to DAPI nuclear counterstaining (blue), in a stromal area of human GBM (scale bar, 50 µm). Bottom panel shows a higher magnification (scale bar, 10 µm). Cellular expression of MHCII highly corresponds to the cellular expression of Iba-1 by microglia and homed macrophages.

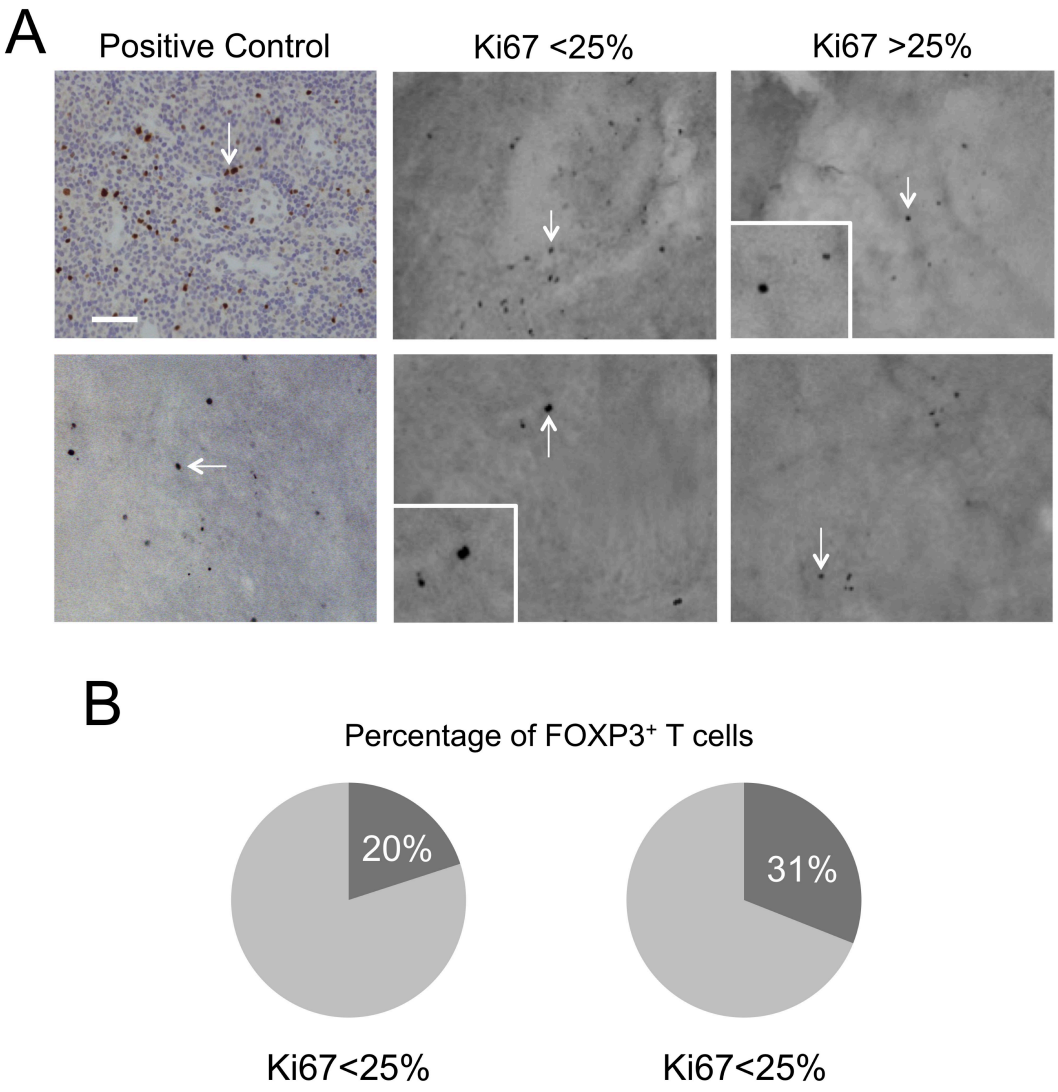

Figure S7. Tumors show FOXP3⁺ regulatory T cells being higher percentage in aggressive GBMs. A. Evidence by immunohistochemistry of FOXP3⁺ T cells in human GBM samples according to the Ki67 percentage. Positive controls are depicted on the left, in top image (sent by the manufacturer) and bottom image (tuberculoma). Arrows indicate examples of positive nuclei. Scale bar: 50 μm. **B.** Percentage of FOXP3⁺ T cells according to Ki67 percentage.

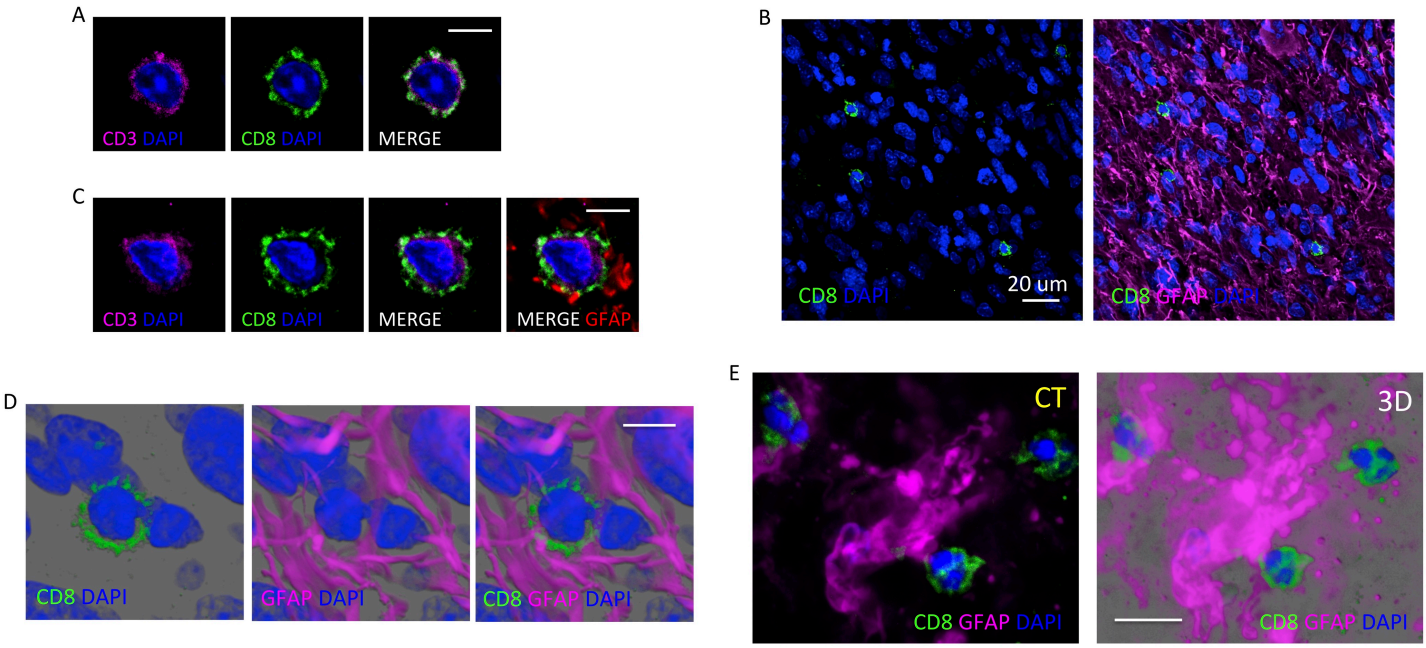

Figure S8. CTLs are present in malignant areas of human GBMs. A. Confocal imaging of CD3 (magenta) and CD8 (green), with DAPI counterstaining (blue) demonstrates that CD8$^+$ T cells co-express CD3 within the human GBM. Scale bar: 10 µm. **B.** Confocal image of a human GBM biopsy containing infiltrated CD8$^+$ T cells in a GFAP-rich malignant area. **C.** CTLs (CD3$^+$/CD8$^+$ T cells) interact with GFAP$^+$ cells (red) within the human GBMs. Scale bar: 10 µm. **D.** 3D reconstruction of a CD8$^+$ T cell (green) interacting with GFAP$^+$ cells (magenta). Nuclei are stained with DAPI (blue). Scale bar: 10 µm. **E.** Confocal transparency (CT) and 3D reconstruction of CD8$^+$ T cells interacting with GFAP$^+$ cells show kinaptic morphology of lymphocytes. Scale bar: 20 µm.

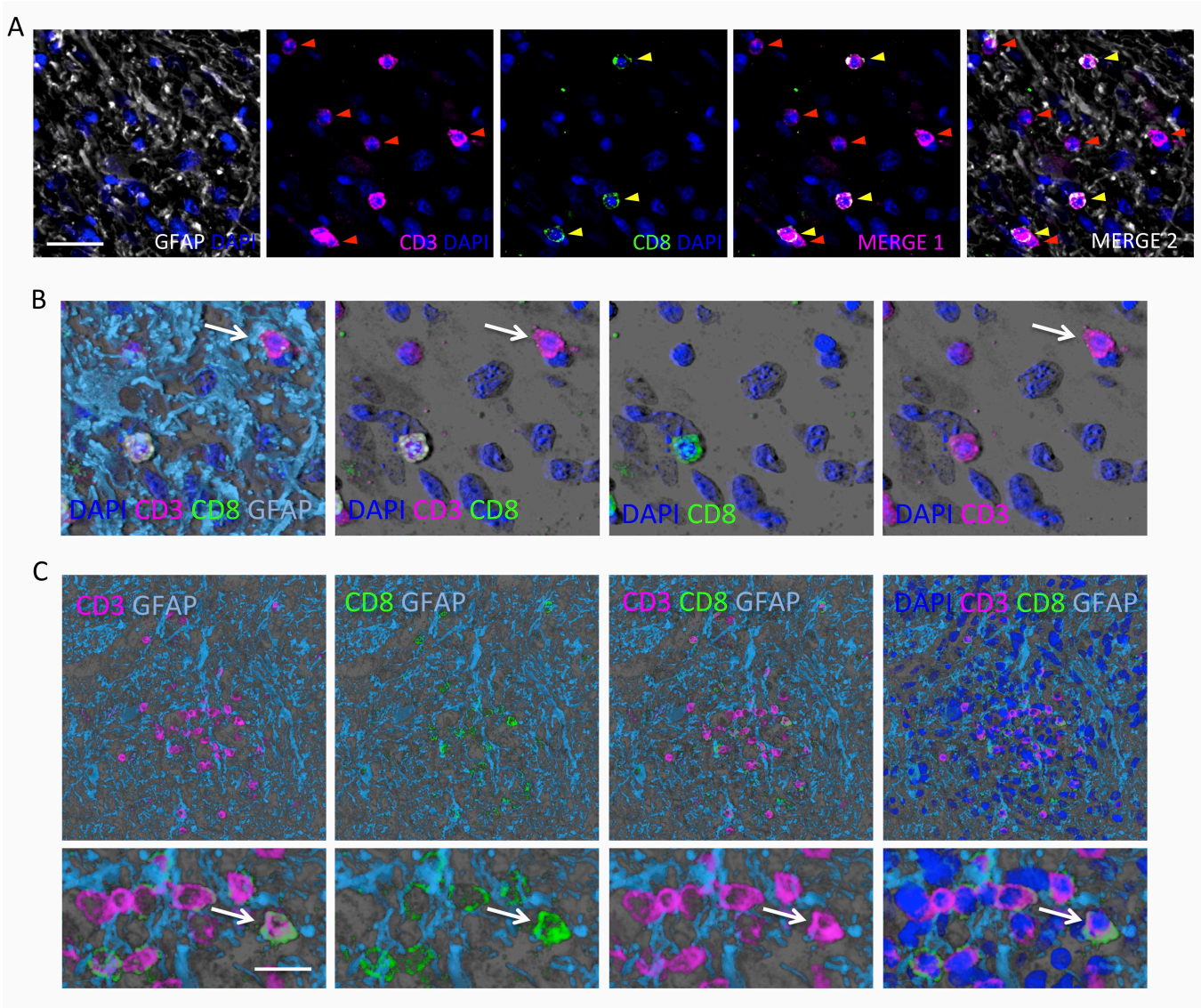

Figure S9. Both CTLs and non-CTLs are present in malignant areas of human GBMs. A. Both CTLs ($CD3^+/CD8^+$) (yellow arrowheads) and non-CTLs ($CD3^+/CD8^-$ cells) (red arrowheads) populate malignant GFAP-rich areas (grey). Scale bar: 30 µm. **B.** 3D reconstruction from cells imaged in panel A revealed kinaptic shape of non-CTLs ($CD3^+/CD8^-$) (white arrow) in $GFAP^+$ areas (cyan). **C.** 3D reconstruction demonstrates kinaptic shape of CTLs ($CD3^+/CD8^+$) (white arrow) in $GFAP^+$ areas (cyan). Scale bar: 20 µm.

Supplemental Videos Legends

Video 1. 3D tissue block transparency containing tumor cells, marked with GFAP (magenta), and T-cells stained against CD3 (green). Rotation of the reconstruction allows the observation of the three-dimensional distribution of T cells within the tumorigenic malignant tissue.

Video 2. 3D tissue block transparency containing stromal cells, marked with MHCII (red), and T-cells stained with CD3 (green). Rotation allows the observation of the three-dimensional distribution of T cells within the tumorigenic stromal tissue.

Video 3. Rotation, zoom-in and clipping plane along z-axis of a 3D rendering of a T-cell establishing a synapsing contact with a glioma cell in human GBM.

Video 4. Rotation, zoom-in and clipping plane of a 3D rendering of a confocal image in which a T-cell is establishing a synapsing contact with a $MHCII^{+}$ cell in human GBM.

Video 5. 3D tissue block transparency. Rotation and zoom-in of a bona-fide IK in a malignant area of a human tumor.

Video 6. 3D reconstruction of a bona-fide IK. Rotation of a T cell with kinaptic shape in a malignant area of a tumor is shown. Isosurfaces of nuclei and CD3 were performed distinguishing high and low CD3 green fluorescence. Importantly, differential expression of CD3 can be distinguished along the structure of the cell. An architecture compatible with a leading lamellipodium and a CD3 rich trailing uropod.

Ref. Manuscript JCI Insight **120757**

Supplemental Material

Table. Characteristics of the glioma samples used. OD; Oligodendroglioma, A; Astrocytoma, AnOD; Anaplastic Oligodendroglioma, GA, gemistocytic astrocytoma, GBM; Glioblastoma Multiforme. FL; Frontal lobe, FIL; Fronto-insular lobe, PL; Parietal lobe, TL; Temporal lobe, FTL; Fronto temporal lobe, IL; Insular lobe.

Patient ID	Glioma Grade	Diagnosis	% of Ki67 Expression	Brain Location
Patient 1	2	OD	2.5%	FL
Patient 2	2	A	5%	FL
Patient 3	4	GBM	5%	FIL
Parient 4	2	GA	10%	PL
Patient 5	2	A	10%	TL
Patient 6	4	GBM	10%	FTL
Patient 7	4	GBM	20%	FTL
Patient 8	4	GBM	20%	FL
Patient 9	4	GBM	20%	PL
Patient 10	4	GBM	24%	FL
Patient 11	4	GBM	30%	IL
Patient 12	4	GBM	30%	TL
Patient 13	4	GBM	30%	TL
Patient 14	4	GBM	50%	FTL
Patient 15	4	GBM	50%	FTL